Tuning electronic and magnetic properties of SnSe$_2$ armchair nanoribbons via edge hydrogenation

Yucheng Huang*, Chongyi Ling, Hai Liu, Sufan Wang.

Center for Nano Science and Technology, College of Chemistry and Material Science, The Key Laboratory of Functional Molecular Solids, Ministry of Education, Anhui Laboratory of Molecule-Based Materials, Anhui Normal University, Wuhu, 241000, Peoples' Republic of China

Abstract: First-principle calculations were carried out to investigate the electronic and magnetic properties of SnSe$_2$ armchair nanoribbons (ANRs) via edge hydrogenation. Interestingly, at different hydrogenation degrees, SnSe$_2$ ANRs exhibit versatile electronic and magnetic properties, i.e., from nonmagnetic-semiconductor to magnetic-semiconductor or nonmagnetic-metal. Through the analysis from spatial spin distribution and density of states, these transitions are well interpreted. Moreover, the relative stabilities of these ANRs were evaluated by the thermodynamic phase diagram where the Gibbs free energies as a function of the chemical potential of H$_2$ molecule at different temperatures were plotted. Our results show that hydrogenation is a well-controlled way to modify the physical properties of SnSe$_2$ ANRs. Through controlling chemical potential or partial pressure of H$_2$, the different hydrogenation degree of ANRs are thermodynamically stable, thus, one can arbitrarily steer its electronic and magnetic properties. The diverse electronic phases and magnetic properties endow the hydrogenated SnSe$_2$ ANRs having potential applications in nanoelectronics.

KEYWORDS First-principle; Tin diselenide; armchair nanoribbon; magnetism; hydrogenation; electronic structure

---

* E-mail: huangyc@mail.ahnu.edu.cn.

1. Introduction

Because of the promising applications in the fields of transistors,[1-3] catalysis,[4] optoelectronic devices[5-7] and energy storage,[8-10] in recent years, the two-dimensional structures of layered chalcogenide materials (LCMs) have been received considerable attention. A single layer of the LCMs always possess a graphene-like structure in which a layer of cationic atom is sandwiched between two layers of the anionic atom. The cationic-sandwich layer bounds tightly internally and interacts with neighboring LCMs layers through weak van der Walls interactions. Different from graphene whose constituent is limited to be carbon atoms, the versatile compositional and structural varieties enable LMCs owning abundant physicochemical properties.

As a typical compound of LCMs family, $SnSe_x$ (x = 1, 2) were proved to have brilliant application prospects due to their excellent optical and electrical properties, i.e, lithium ion batteries,[11] infrared optoelectronic devices, solar cells,[12] phase change memory[13] as well as other optical devices.[14, 15] Unlike the case of graphene whose derived one-dimensional (1D) nanoribbons/nanotubes exhibit various properties depending on their width and chirality, [16-22] 1D $SnSe_2$ nanostructures always display a monotonous nonmagnetic semiconducting or nonmagnetic metallic property,[23-25] which may result in the wider applications being constrained. Therefore, investigation of the way to tune the physical properties (i.e., electronic structure and magnetism) becomes pressingly needed. We demonstrated recently that strain engineering offer effective tuning of electronic and magnetic properties in $SnSe_x$ nanostructures,[23, 24] which would make the potential applications be extended to nanoelectronics,

nanoelectromechanical devices, and spintronics.

Besides exerting strain, chemical functionalization and applying external electric field are the other viable methods. Hydrogenation stands out since many theoretical and experimental studies revealed that the electronic and magnetic properties of nanostructures can be well tuned by hydrogenation,[26-34] and the complete or selective hydrogenation have already realized in laboratory. By means of the first-principles calculations, Sofo et al.[26] unveiled that fully hydrogenated graphene (graphane) has a wide energy gap which is different to the original graphene and has potential application in hydrogen storage. They also discussed the possible route for synthesizing graphane. Very shortly after this, graphane was indeed realized in labs, and proved to be an electronic insulator.[27, 28] Moreover, the fully and partially hydrogenated graphene nanoribbons (GNRs) have also been respectively studied by Li et al.[29] and Xiang et al.[30] The results showed that the fully hydrogenated GNRs are nonmagnetic semiconductors with a wide energy gap, while the partially hydrogenated ones have similar magnetic and electronic properties as those of the narrow ones representing their graphene parts, which provide a possible way to obtain the narrow GNRs in large scale. Besides 2D graphene and its derived 1D nanoribbons, recent studies are extended to other inorganic nanostructures, including LCMs. For example, hydrogenation was proved to be an effective method to steer the electronic and magnetic properties of boron nitride (BN) nanostructures.[31-34] Chen et al. [31] found that the semiconductor-half metal-metal transition can be realized in BN zigzag nanoribbons (ZNRs) with different hydrogenation degrees. Moreover, the

one-H-terminated BNNRs are nonmagnetic[33], while the two-H-terminated BN ZNRs are magnetic.[34] For LCMs, the explosion of theoretical and experimental investigations has recently occurred on MoS_2, especially the discoveries of its interesting electronic and magnetic properties. The 2D MoS_2 monolayer has been proved to be a direct-gap semiconductor by both experiments[35] and theoretical computations.[36] Partial hydrogenation on the surface of MoS_2 monolayer can trigger the semiconductor-metal transition[37] and the fully hydrogenated one can induce the nonmagnetic-magnetic transition by applying strain.[38]

Inspired by the studies concerning hydrogenation on the nanostructures as described above, naturally, some questions arise: How about the effect of hydrogenation on the electronic properties of $SnSe_2$ nanostructures? Whether the magnetic behavior can be induced by hydrogenation? Do hydrogenation degrees have effect on the electronic and magnetic properties? To uncover these questions, in this contribution, we systematically studied the electronic and magnetic properties of $SnSe_2$ armchair nanoribbons (ANRs) with different forms of edge hydrogenation by means of the first-principles calculations. Here the $SnSe_2$ ANR is chosen as prototype, which is based on the two considerations. First, our previous study demonstrated that a semiconductor-magnetic metal can be realized in $SnSe_2$ ANRs when subjected to a -10% compressive strain.[24] The interesting findings intrigue us to dig deeply into its physical properties. More important, our preliminary calculations showed that the electronic and magnetic properties of other 1D $SnSe_2$ nanostructures (zigzag nanoribbons and nanotubes) are not pronounced changed via hydrogenation. Our

results disclose that the nonmagnetic semiconductor of the SnSe$_2$ ANRs can transform into magnetic semiconductor or nonmagnetic metal depending on the hydrogenation degrees. The calculated Gibbs free energies show that the anions of Se atom are preferably hydrogenated within a large scope of H$_2$ partial pressure (p). Hydrogenation on Sn atom occurs at the extremely high pressure of 3.6×10^{26} bar at the temperature (T) of 298.15 K or p = 7.7×10^{16} bar at T = 600 K. Conclusively, we demonstrate that through controlling the hydrogenation degree (determined by the chemical potential or partial pressure of H$_2$), one can artificially modulate the electronic and magnetic properties of SnSe$_2$ ANRs. We believe that our results may provide SnSe$_2$ to be applicable in the nanoelectronics.

2. Computational Details

The generalized gradient approximation (GGA) in the Perdew−Burke−Ernzerhof (PBE) form[39, 40] and a 350 eV cutoff for plane-wave basis set were adopted as implemented in the Vienna ab initio simulation package (VASP).[41, 42] The projector-augmented plane wave (PAW)[43] method was employed to model the ion-electron interaction. $5s^2 5p^2$ electrons states of Sn atom, $4s^2 4p^4$ electrons states of Se atom and $1s^1$ electron state of H atom were considered as valence electrons. The convergence threshold was set to 1×10^{-5} eV and 2×10^{-2} eV/Å for energy and force, respectively. To avoid the interaction between two periodical units, the vacuum space at least 12 Å is adopted. Various ANRs (e.g., 8-, 10- and 14-ANR) with different width were considered and the results showed that the width of ribbon has minor

effect on the electronic and magnetic properties at different hydrogenation degrees. Thus, for the sake of convenience, only $SnSe_2$ 10-ANR was selected in this work, corresponding to the width of approximate 18 Å. For the geometric and electronic structural calculations, the Brillouin zone sampling was using 6 Monkhost-Pack[44] k points grid. On the basis of the equilibrium structures, 21 k points were then used to compute the electronic band structures. The energy cutoff and k-points settings are proved to be sufficient for achieving converged results.[24, 25] Over the computations, both spin-unpolarized and spin-polarized calculations were performed to determine the ground state. To find the magnetic ground state of the $SnSe_2$ ANRs, a supercell with two repeating units containing 2 $SnSe_2$ molecule units along the edge is used. For each magnetic NRs, two kinds of calculations were performed to investigate the possible magnetism: ferromagnetic (FM) and antiferromagnetic (AFM), which is dependent on the initial conditions of the self-consistent calculations. Note that semilocal (local density approximation (LDA) and GGA) exchange-correlation functionals typically underestimate the experimental band gap. However, the goal of this work is not to pursue the exact band gap but to illustrate the phenomenon of gap tuning via edge hydrogenation. The systematic underestimation of band gaps by semilocal functionals would not change the underlying physics and regularity.

3. Results and Discussion

Because each edge has two unsaturated Se atoms and one unsaturated Sn atom in the unit cells of 10-ANRs, ten possible hydrogenated $SnSe_2$ ANRs structures were

thereby constructed, which are illustrated in Figure 1. The ten hydrogenated $SnSe_2$ ANRs can be divided into two categories: one is depicted in Figure 1a-1f, where only Sn or Se atoms are hydrogenated; and the other is seen in Figure 1g-1j, where Sn and Se are simultaneously hydrogenated. For the convenience of discussion, the hydrogenation degree is denoted as the ratio of H to the edge Sn or Se atoms. For example, Sn50%-Se0% represents 50% Sn whereas no Se atoms are hydrogenated.

3.1 Hydrogenation on edge Sn sites

Because of having chemically nonequivalent Sn and Se atoms, the semihydrogenation can be achieved by merely saturating either the Sn sites or the Se sites. As seen in Figure 1, there are two Sn atoms distributing onto two edges, that is, each edge has one Sn atom. Therefore, two models named Sn50%-Se0% and Sn100%-Se0%, are designed as shown in Figure 1a and 1b, respectively.

The Sn-H bond length is calculated to be 1.73 Å on both two structures. According to Bader charge analysis,[45] we found a 0.24 e/atom charge transferring from Sn to the H, indicative of the negative charged of H. The electrons lose of Sn accompanies with the elongation of Sn-Se bond length in the edge.

To determine whether these two hydrogenated $SnSe_2$ ANRs have magnetism or not, both spin-unpolarized and spin-polarized calculations were preformed. Once the magnetism is verified, further calculations need to be done to determine the stable magnetic structures (i.e., FM and AFM). To investigate the magnetic couplings, we doubled the size of the supercell along the edge direction, such that each edge now

contains two SnSe$_2$ units, and the distance between two adjcent Sn atoms is about

6.7 Å. The energies of NM (E_{NM}), FM (E_{FM}) and AFM (E_{AFM}) couplings are tabulated

in Table 1, at which the energies not listed are nonmagnetic structures. It clearly

shows that the FM states are the most stable as they have the lowest energy (E_{FM}). The

energy differences between NM and FM state ($\Delta E_{NM\text{-}FM}$) for Sn50%-Se0% and

Sn100%-Se0% are 174.28 and 348.39 meV, respectively, demonstrating that the

spin-polarized states are relatively stable. However, the energy differences between

FM and AFM are always minute (within 2 meV), demonstrating an easy spin-flipping

for the magnetic atoms and essentially the same probability occurrence of these two

magnetic states.[46]

The band structures were also calculated as exemplified in Figure 2. It can be seen

that both structures are FM semiconductors with a moderate indirect energy gap. For

Sn50%-Se0%, the energy gaps are 0.67 and 0.59 eV in the majority spin and minority

spin states, respectively. These values increase to 0.72 and 0.71 eV when two edge Sn

atoms are simultaneously hydrogenated. The band gap varies with the hydrogenation

degree, which can be regarded as a promising way to modulate the band gap. The

adsorption of each H atom on edge Sn site introduces one low acceptor level located

above the valence band minimum (i.e., from II in majority spin to I in minority spin as

shown in Figure 2a and from I to I in Figure 2b), leading to the spin polarization with

one spin channel completely occupied. Typically, the adsorbed H should act as an

n-doping source due to an electron donator character. However, the direction of

electron transfer is from Sn to the H atom, resulting in hole-doping p-type

semiconductivity and inducing total magnetic moment of 1.00 μ_B (Table 1). Similar

phenomenon was also found in the hydrogenated single layered ZnO nanosheet.[47]

To have a deeper insight into the origin of the induced magnetism, the

spin-polarized partial density of states (PDOS) and spatial spin distributions are

illustrated in Figure 3. In fact, pristine $SnSe_2$ ANRs have no magnetism[25] while

hydrogenation on Sn atoms forms strong Sn-H bonds, leaving the dangling bonds of

edge Se atoms spin unpaired. It's evident that the unpaired spin completely

concentrates on the edge Se atom and contributed by the 4p electrons (Figure 3).

H-induced spin polarization can be understood from the variation of Sn-Se bond

length and the variation of edge Sn atom charge. The increased Sn-Se bond length

(from 2.51 to 2.76 Å) via hydrogenation would result in the reduction in the covalent

bond strength and the enhancement in the ionic bonding interaction, thus giving rise

to the unpaired electrons accumulating. This analysis is in accord with the result from

Bader charge calculation. It is found that edge Sn atom carries 2.90 electrons on the

pristine ANR, but decreases to 2.80 electrons on the Sn50%-Se0% and Sn100%-Se0%.

The magnetism entirely originates from the nonmetallic anion, resembling to the

scenario with applying a -10% compressive strain.[24]

3.2 Hydrogenation on edge Se sites

As illustrated in the Figure 1, the edges of $SnSe_2$ ANR have four Se atoms.

Accordingly, four hydrogenated structures were constructed named Sn0%-Se25%,

Sn0%-Se50%, Sn0%-Se75% and Sn0%-Se100%, as shown in Figure 1c to 1f. It is

worth noting that, there is more than one possible configuration for Sn0%-Se50% and Sn0%-Se75%. Here, we only consider the most stable one as consolidated in the Figure 1d and 1e. All the calculated Se-H bond lengths are 1.49 Å, which are somewhat slightly longer than the ones in SeH_2 gas phase (Expt., 1.46),[48] indicative of the strong bonding strength.

The calculated electronic properties, which are dependent on the hydrogenation degrees, can be divided into two categories as shown in Figure 4, that is, magnetic-semiconductor for Sn0%-Se25% and Sn0%-Se75%, and nonmagnetic-semiconductor for Sn0%-Se50% and Sn0%-Se100%.

In Table 1, we tabulated the calculated energies, which show that the FM coupling is the ground state for Sn0%-Se25% and Sn0%-Se75% and NM for the remaining ones. Similar to the scenarios of hydrogenation on Sn site, 25% and 75% Se hydrogenations present indirect energy gaps in both spin-up and spin-down states. The energy gaps in spin-up and spin-down states are 0.35 and 0.52 eV for Sn0%-Se25% and 0.43 and 0.54 eV for Sn0%-Se75%, respectively. Also one can see the energy gaps change with the hydrogenation degree. For Sn0%-Se50% and Sn0%-Se100%, the indirect energy gaps are calculated to be 0.69 and 0.77 eV, respectively.

Similar to the hydrogenation on Sn atoms, the band structures of Sn0%-Se25% and Sn0%-Se75% display hole-doping p-type semiconductivity as one low acceptor level of majority spin transfers to high donor level of minority spin (Figure 4). This phenomenon is also in agreement with the Bader charge analysis, at which

approximate 0.05 e/atom charge is found to transfer from Se to H, as a result, the

Sn-Se bond length on the edge is elongated. The redundant electron delocalizes on the

SnSe$_2$ edge, resulting in spin polarization.

To understand the diverse electronic and magnetic properties of SnSe$_2$ ANR with

different hydrogenation degrees on the edge Se atoms, the PDOS and spatial spin

distributions are plotted in Figure 5. Interestingly, different from the cases under -10%

compressive strain[24] or hydrogenation on edge Sn sites whose magnetism is

completely contributed by edge Se atoms, the induced magnetism is attributed

primarily to the unsaturated edge Se and edge Sn sites, with a little contribution from

Se atoms near the edge (Figure 5), indicative of a large spatial distribution. The Se

atoms process a ~ 0.29 μ_B magnetic moment, while the Sn atom carries a magnetic

moment of ~ 0.30 μ_B, leading to the total magnetic moment of ~ 1 μ_B (Table 1). PDOS

analysis shows that the unpaired spin concentrates on the edge Se atoms 4p electrons

and Sn atoms 5s and 5p electrons.

It is interesting that 50% and 100% Se atoms hydrogenation would not induce

magnetism. When one H atom is hydrogenated, strong σ-bonds are formed between H

and Se atoms, resulting in the electrons in the unhydrogenated Sn and Se atoms

becoming localized and spin-polarized. When two Se atoms at the same edge are

simultaneously hydrogenated, the length of edged Sn-Se bond further stretches, and

finally cracks (Figure 1). It was shown that one H adsorption makes the electron be

accumulated on Sn atom, which can be understood as Sn may save "one" electron to

contribute Sn-Se bond. As two H atoms adsorb on Se atoms, "another" electron is

excess on Sn atom, and these "two" electrons may be paired, leading to spin-unpolarization.

3.3 Hydrogenation on edge Sn and Se sites simultaneously

There are too many combinations when H-atoms simultaneously distribute onto edge Sn and Se atoms. To simplify computations and decrease the computational burdens, here only half of Sn, Se and complete Sn, Se atom hydrogenations were taken into account. Note that different from hydrogenation on only Sn atoms, there are two H-adsorption modes on Sn when both Sn and Se atoms are hydrogenation, i.e., one H and two H atoms adsorption (Figure 1). Therefore, four structures named Sn50%Se50%, Sn100%Se100%, Sn50%(di)Se50% and Sn100%(di)Se100% are designed as shown in Figure 1g to 1j. Here, "di" means Sn atom connects to two H atoms. For example, Sn50%(di)Se50% denotes a half of Se and a half of Sn atoms are hydrogenated, and the Sn atom connects to two hydrogen atoms. It is to be noted that only four configurations chosen here will not affect the conclusions that diverse electronic and magnetic properties are associated with different hydrogenation degrees (see below).

For Sn50%Se50%, there is also more than one configuration, i.e., hydrogen can adsorb on either one edge or both edges. Our test calculations show that at the same hydrogenation coverage, the configuration of one side hydrogenation is energetically favorable than the one of arbitrary hydrogenation, which is consistent with the case for BN nanoribbon.[31] For Sn50%Se50% and Sn100%Se100%, the calculated Sn-H

and Se-H bond lengths are 1.73 and 1.49 Å, respectively, which are essentially the same as those of hydrogenation on only Sn and only Se sites. For Sn50%(di)Se50% and Sn100%(di)Se100%, the Se-H bond lengths are also 1.49 Å while the Sn-H bond lengths increase to 1.75 Å. The elongation of Sn-H bond is corroborated by the charge transfer: for monohydrogenation on Sn atom, 0.26 electrons transfer from Sn to the H atom; for dihydrogenation, 0.29 electrons transfer from Sn to each H atom.

Subsequently, the electronic and magnetic properties of these hydrogenated SnSe$_2$ ANRs were studied. All the hydrogenated ANRs were proved to be nonmagnetic because the spin-unpolarized energies are always lower than the spin-polarized ones. Figure 6 shows the calculated electronic structures of these four configurations. For Sn50%Se50% and Sn100%Se100%, there are partial occupied electron states across the Fermi level, indicating of a metallic character. To confirm the correctness of the physical description, the hybrid HSE06 functional is used.[49] The result shows it is still a metal, demonstrating the qualitative description by GGA/PBE is valid. For Sn50%(di)Se50% and Sn100%(di)Se100%, the Fermi level locates within the limits of forbidden band, which is the typical feature of semiconductor, and the indirect energy gaps are calculated to be 0.66 and 0.99 eV for Sn50%(di)Se50% and Sn100%(di)Se100%, respectively. Previous studies predicted the fully hydrogenated graphene and monolayer BN sheets as well as one-bilayer ZnO sheet are nonmagnetic semiconductor, similar to the conclusion drawn on SnSe$_2$ ANR with deep hydrogenation.[26, 47, 50] The total density of state (TDOS) analysis is in accordance with the energy band calculations. As seen in Figure 7, the electronic states of

Sn50%Se50% and Sn100%Se100% cross over the Fermi level, while those of Sn50%(di)Se50% and Sn100%(di)Se100% do not.

In the context, we always put an emphasis on the viewpoint that the bond length is strongly associated with the balance between ionic bonding and covalent interaction and meanwhile, this balance is closely related to the charge transfer. Taking hydrogenation on both edge Sn and Se sites as examples, we can demonstrate it from PDOS analysis. From Figure 7, we found that some small peaks locate within the range from -6.0 to -5.5 eV (for monohydrogenation, see Figure 7a and 7b) and from -5.5 to -4.5 eV (for dihydrogenation, see Figure 7c and 7d) on TDOS, which is contributed by the coupling between edge Se atom p orbital, edge Sn atom p orbital and H s orbital. These peaks do not appear in pure $SnSe_2$ ANRs[25] and the inner site of hydrogenated $SnSe_2$ ANRs (not shown), indicating that it originates from the Se-H and Sn-H bondings. From monohydrogenation to dihydrogenation over Sn atoms, the state of H atom at these regions is significantly reduced, demonstrating the reduction in the covalent bonding interaction and simultaneously, the enhancement in the ionic bonding interaction. As a result, the Sn-H bond lengths will increase (from 1.64 to 1.75 Å).

3.4 Stabilities of the hydrogenated $SnSe_2$ ANRs

Finally, we plot the Gibbs free energy (G_{H_2}) as a function of the chemical potential of H_2 molecule (μ_{H_2}) at different temperatures (100, 298.15 and 600 K) to evaluate the possibility of experimental realizations according to the following formulae[51, 52]

$$G_{H_2} = E_f - \frac{1}{2}\rho_H \mu_{H_2} \qquad (1)$$

in which the formation energy per length E_f and μ_{H_2} are respectively defined as

$$E_f = \frac{1}{2L}(E_{H-NRs} - NE_{SnSe_2} - \frac{N_H}{2}E_{H_2}) \qquad (2)$$

$$\mu_{H_2} = H°(T) - H°(0) - TS°(T) + k_B T \ln(\frac{p_{H_2}}{p°}) \qquad (3)$$

the edge hydrogen density $\rho_H = \frac{N_H}{2L}$, L is the periodic length of SnSe₂ NRs. $E_{H-NRs}, E_{SnSe_2}, E_{H_2}$ are the energies of hydrogenated NRs, SnSe₂ unit and H₂ molecule, respectively. The energy of SnSe₂ unit is achieved from SnSe₂ monolayer. $H°/S°$ is the enthalpy/entropy of H₂ molecule at the pressure $p° = 1$ bar which is adopted from reference.[53] p_{H_2} is the partial pressure of H₂. The calculated Gibbs free energies versus chemical potential or pressure of H₂ molecule is plotted in Figure 8. It can be seen that hydrogenation on Se atoms is always preferable within a large scope of p_{H_2}. When $\mu_{H_2} \leq$ -1.11 eV, hydrogenation of 25% Se is the most stable; when -1.11 $\leq$ $\mu_{H_2} \leq$ -0.41 eV, hydrogenation of 50% Se is the dominant configuration and when μ_{H_2} is in the range of -0.41 to 1.25 eV, 100% Se atoms are preferably hydrogenated. If μ_{H_2} continuously increases, hydrogenation begins to occur on the cation of Sn atom. However, this corresponds to an extremely large p_{H_2} of 3.6×10²⁶ bar at the room temperature. It can be significantly decreased to 7.7×10¹⁶ bar when temperature rises to 600 K and this value will be further reduced with the temperature increasing. It should be noticed that, at ambient conditions (where the partial H₂ pressure in air is ~5×10⁻⁷ bar) and room temperature, the most stable structure is the nonmagnetic Sn0%-Se50%; when T increases to 600 K, the magnetic Sn0%-Se25% becomes the most stable one; and the nonmagnetic Sn0%-Se100% can be produced when T

decreases to 100 K. On the other hand, at a certain temperature, the different

hydrogenation degree can be also captured by varying partial pressure of H_2.

Conclusively, from our thermodynamic analysis, hydrogenation on Se is always

preferred. Through controlling μ_{H_2} or P_{H_2} (T), one can arbitrarily manipulate the

electronic and magnetic properties of $SnSe_2$ ANRs.

Although our phase diagram vividly indicates that Se sites are preferably

hydrogenated as a general rule, one can not deny that hydrogenation on Sn site may

be feasible on the laboratory. A possible synthesis strategy, for example, is firstly

through passivation of Se site, and then deprotects Se site after hydrogen adsorbs on

Sn. Therefore, investigation of hydrogenation on the Sn site not only can provide

useful and comprehensive information on the various physical properties of $SnSe_2$

ANR, but also can fully excavate their possible potential applications in nanodevices.

4. Conclusion

In summary, comprehensive investigations on the electronic and magnetic properties

of $SnSe_2$ ANRs with different hydrogenation degrees were carried out by means of the

first-principles calculations. Our results unveil that the nonmagnetic semiconductor of

$SnSe_2$ ANRs can transform into magnetic semiconductor or nonmagnetic metal,

depending on the hydrogenation degrees. The computation of Gibbs free energy as a

function of the chemical potential of H_2 molecule shows that hydrogenation on Se

atom is preferred while hydrogenation on Sn site need a harsh condition, and thus, our

result opens a novel way to modulate the electronic and magnetic properties of $SnSe_2$

ANRs, which would provide useful information to their potential applications and would stimulate further experimental and theoretical investigations toward LCMs and its derived 1D nanostructures.

References

1. M. Osada and T. Sasaki, *Adv. Mater.*, 2012, **24**, 210.
2. B. Radisavljevic, A. Radenovic, J. Brivio, V. Giacometti and A. Kis, *Nat. Nanotechnol.*, 2011, **6**, 147.
3. J. Pu, Y. Yomogida, K.-K. Liu, L.-J. Li, Y. Iwasa and T. Takenobu, *Nano Lett.*, 2012, **12**, 4013.
4. K. H. Hu, X. G. Hu, Y. F. Xu and X. Z. Pan, *React. Kinet. Mech. Cat*, 2010, **100**, 153.
5. A. Splendiani, L. Sun, Y. Zhang, T. Li, J. Kim, C.-Y. Chim, G. Galli and F. Wang, *Nano Lett.*, 2010, **10**, 1271.
6. H. S. Lee, S.-W. Min, Y.-G. Chang, M. K. Park, T. Nam, H. Kim, J. H. Kim, S. Ryu and S. Im, *Nano Lett.*, 2012, **12**, 3695.
7. M. Thomalla and H. Tributsch, *J. Phys. Chem. B*, 2006, **110**, 12167.
8. A. M. Seayad and D. M. Antonelli, *Adv. Mater.*, 2004, **16**, 765.
9. J. Liu and X. W. Liu, *Adv. Mater.*, 2012, **24**, 4097.
10. K. Chang and W. Chen, *Chem. Commun.*, 2011, **47**, 4252.
11. J. Choi, J. Jin, I. G. Jung, J. M. Kim, H. J. Kim and S. U. Son, *Chem. Commun.*, 2011, **47**, 5241.
12. K. John, B. Pradeep and E. Mathai, *J. Mater. Sci.*, 1994, **29**, 1581.
13. R. Y. Wang, M. A. Caldwell, R. G. D. Jeyasingh, S. Aloni, R. M. Shelby, H.-S. P. Wong and D. J. Milliron, *J. Appl. Phys.*, 2011, **109**, 113506.
14. S. Liu, X. Guo, M. Li, W. H. Zhang, X. Liu and C. Li, *Angew. Chem., Int. Ed.*, 2011, **50**, 12050.
15. W. J. Baumgardner, J. J. Choi, Y.-F. Lim and T. Hanrath, *J. Am. Chem. Soc.*, 2010, **132**, 9519.
16. Y.-W. Son, M. L. Cohen and S. G. Louie, *Phys. Rev. Lett.*, 2006, **97**, 216803.
17. Y.-W. Son, M. L. Cohen and S. G. Louie, *Nature*, 2006, **444**, 347.
18. K. N. Kudin, *ACS Nano*, 2008, **2**, 516.
19. X. Li, X. Wang, L. Zhang, S. Lee and H. Dai, *Science*, 2008, **319**, 1229.
20. K. A. Ritter and J. W. Lyding, *Nat. Mater.*, 2009, **8**, 235.
21. L. Yang, C.-H. Park, Y.-W. Son, M. L. Cohen and S. G. Louie, *Phys. Rev. Lett.*, 2007, **99**, 186801.
22. A. Yamashiro, Y. Shimoi, K. Harigaya and K. Wakabayashi, *Phys. Rev. B*, 2003, **68**, 193410.
23. Y. Huang, C. Ling, H. Liu and S. Wang, *RSC Adv*, 2014, **4**, 6933.
24. Y. Huang, C. Ling, H. Liu, S. Wang and B. Geng, *J. Phys. Chem. C*, 2014, **118**, 9251.
25. Y. Huang, C. Ling, Z. Fang and S. Wang, *Phys. E*, 2014, **59**, 102.
26. J. O. Sofo, A. S. Chaudhari and G. D. Barber, *Phys. Rev. B*, 2007, **75**, 153401.
27. D. Elias, R. Nair, T. Mohiuddin, S. Morozov, P. Blake, M. Halsall, A. Ferrari, D. Boukhvalov, M. Katsnelson and A. Geim, *Science*, 2009, **323**, 610.
28. S. Ryu, M. Y. Han, J. Maultzsch, T. F. Heinz, P. Kim, M. L. Steigerwald and L. E. Brus, *Nano Lett.*, 2008, **8**, 4597.
29. Y. Li, Z. Zhou, P. Shen and Z. Chen, *J. Phys. Chem. C*, 2009, **113**, 15043.
30. H. Xiang, E. Kan, S.-H. Wei, M.-H. Whangbo and J. Yang, *Nano Lett.*, 2009, **9**, 4025.
31. W. Chen, Y. Li, G. Yu, C.-Z. Li, S. B. Zhang, Z. Zhou and Z. Chen, *J. Am. Chem. Soc.*, 2010, **132**, 1699.
32. F. Li, Z. Zhu, M. Zhao and Y. Xia, *J. Phys. Chem. C*, 2008, **112**, 16231.

33.   A. Du, S. C. Smith and G. Lu, *Chem. Phys. Lett.*, 2007, **447**, 181.

34.   Y. Ding, Y. Wang and J. Ni, *Appl. Phys. Lett.*, 2009, **94**, 233107.

35.   K. F. Mak, C. Lee, J. Hone, J. Shan and T. F. Heinz, *Phys. Rev. Lett.*, 2010, **105**, 136805.

36.   S. Han, H. Kwon, S. K. Kim, S. Ryu, W. S. Yun, D. Kim, J. Hwang, J.-S. Kang, J. Baik and H. Shin, *Phys. Rev. B*, 2011, **84**, 045409.

37.   Y. Cai, Z. Bai, H. Pan, Y. P. Feng, B. I. Yakobson and Y.-W. Zhang, *Nanoscale*, 2014, **6**, 1691.

38.   H. Shi, H. Pan, Y.-W. Zhang and B. I. Yakobson, *Phys. Rev. B*, 2013, **88**, 205305.

39.   J. P. Perdew, J. Chevary, S. Vosko, K. A. Jackson, M. R. Pederson, D. Singh and C. Fiolhais, *Phys. Rev. B*, 1992, **46**, 6671.

40.   J. P. Perdew and Y. Wang, *Phys. Rev. B*, 1992, **45**, 13244.

41.   G. Kresse and J. Furthmüller, *Phys. Rev. B*, 1996, **54**, 11169.

42.   G. Kresse and D. Joubert, *Phys. Rev. B*, 1999, **59**, 1758.

43.   P. E. Blöchl, *Phys. Rev. B*, 1994, **50**, 17953.

44.   H. J. Monkhorst and J. D. Pack, *Phys. Rev. B*, 1976, **13**, 5188.

45.   G. Henkelman, A. Arnaldsson and H. Jónsson, *Comput. Mater. Sci.*, 2006, **36**, 354.

46.   X. Zhang, M.-F. Ng, Y. Wang, J. Wang and S.-W. Yang, *ACS Nano*, 2009, **3**, 2515.

47.   Q. Tang, Y. Li, Z. Zhou, Y. Chen and Z. Chen, *ACS Appl. Mater. Interfaces*, 2010, **2**, 2442.

48.   J. Callomon, E. Hirota, K. Kuchitsu, W. Lafferty, A. Maki and C. Pote, *Structure Data on Free Polyatomic Molecules,* Springer, Berlin, 1976, Vol. 7.

49.   J. Paier, M. Marsman, K. Hummer, G. Kresse, I. Gerber and J. Ángyán, *J. Chem. Phys.*, 2006, **125**, 9901.

50.   Y. Wang, *Phys. Status Solidi RRL*, 2010, **4**, 34.

51.   T. Wassmann, A. P. Seitsonen, A. M. Saitta, M. Lazzeri and F. Mauri, *Phys. Rev. Lett.*, 2008, **101**, 096402.

52.   D.-Q. Fang, S.-L. Zhang and H. Xu, *RSC Adv*, 2013, **3**, 24075.

53.   M. Chase Jr, NIST-JANAF Thermochemical Tables, *J. Phys. Chem. Ref. Data*, 4th ed., 1998, Monograph No. 9.

Figures

Figure 1. Structures of the different forms of hydrogenated SnSe$_2$ ANR. The Sn, Se and H atoms

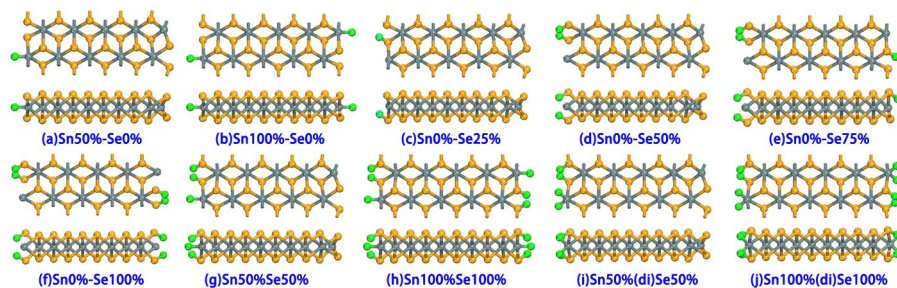are represented by the brown, yellow and green balls, respectively.

(a)Sn50%-Se0% (b)Sn100%-Se0% (c)Sn0%-Se25% (d)Sn0%-Se50% (e)Sn0%-Se75%

(f)Sn0%-Se100% (g)Sn50%Se50% (h)Sn100%Se100% (i)Sn50%(di)Se50% (j)Sn100%(di)Se100%

Figure 2. The band structures and partial charge distribution of (a) Sn50%-Se0% and (b)

Sn100%-Se0%. The blue and green solid lines represent the majority spin and minority spin

components, respectively. The red dashed line represents the Fermi level.
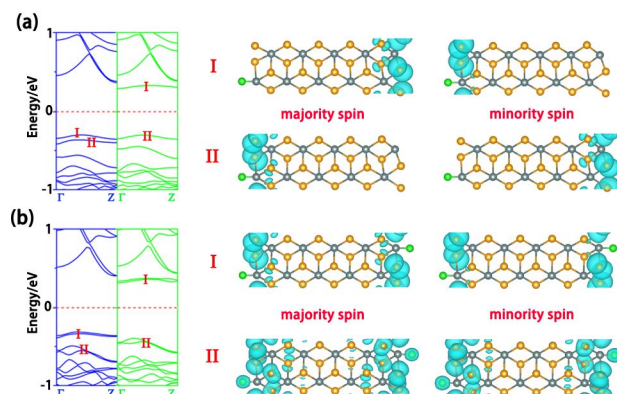
Figure 3. Spin-polarized partial density of states (PDOS) and spatial spin distribution (up-down) of Sn50%-Se0% (a and c) and Sn100%-Sn0% (b and d). The blue and green regions represent the spin-up and spin-down components, respectively. The isosurface is set to be 0.002 e/Å^3.
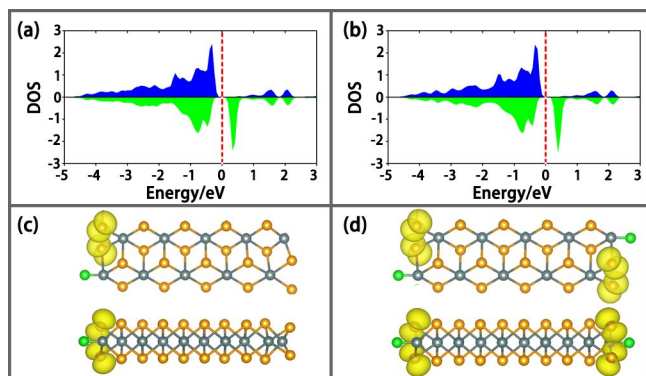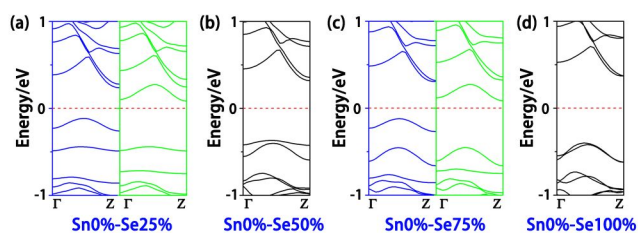

Figure 4. The band structures of (a) Sn0%-Se25%, (b) Sn0%-Se50%, (c) Sn0%-Se75% and (d) Sn0%-Se100%. The blue and green solid lines represent the spin-up and spin-down components, respectively. The red dashed line represents the Fermi level.

Figure 5. Spin-polarized partial density of states of Sn0%-Se25% (a and b) and Sn0%-Se75% (d

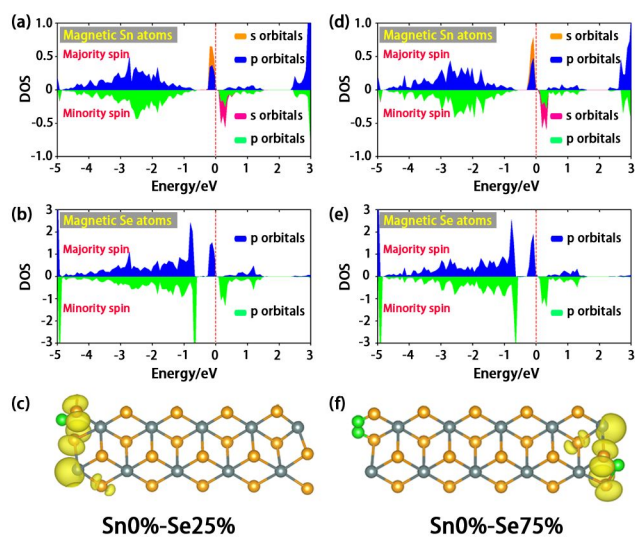and e) and the corresponding spatial spin distribution (c and f).

Figure 6. The band structures of (a) Sn50%Se50%, (b) Sn100%Se100%, (c) Sn50%(di)Se50% and

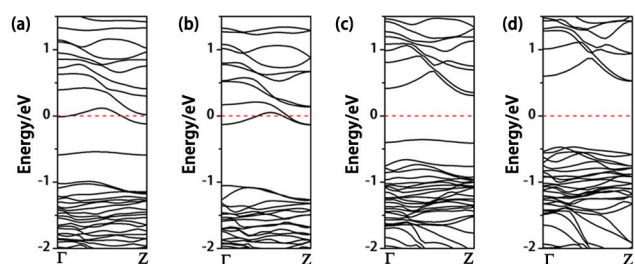(d) Sn100%(di)Se100%. The red dash lines represent the Fermi level.

Figure 7. The TDOS and PDOS of (a) Sn50%Se50%, (b) Sn100%Se100%, (c) Sn50%(di)Se50%

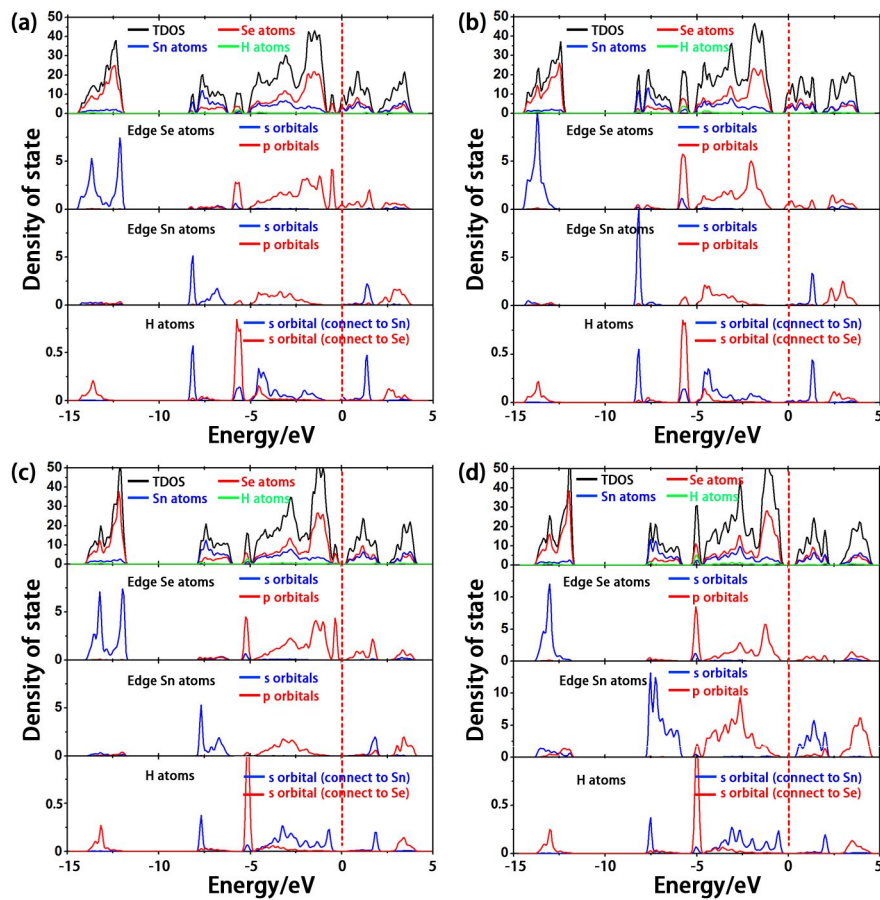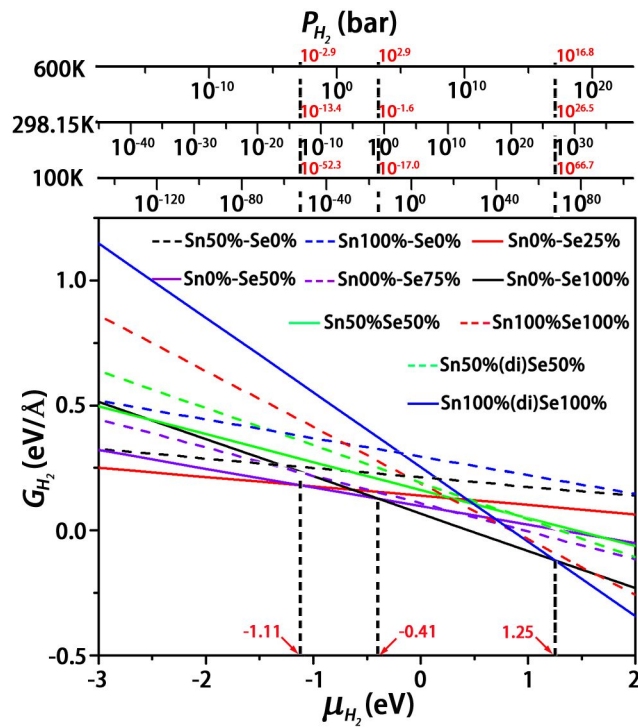and (d) Sn100%(di)Se100%. The red dash lines represent the Fermi level.

Figure 8. Gibbs free energies versus chemical potential and pressure of H_2 molecule for $SnSe_2$

10-ANR with different hydrogenated structures at $T = 100$, 298.15 and 600 K.

Tables

Table 1. The energies of E_{NM}, E_{FM} and E_{AFM} (in eV), and the energy differences (in meV) between E_{NM} and E_{FM} ($\Delta E_{NM\text{-}FM}$), E_{AFM} and E_{FM} ($\Delta E_{AFM\text{-}FM}$), magnetic moments with FM state (μ_B) of four magnetic structures per unit cell (one $SnSe_2$ unit along the growth direction).

Structure	E_{NM}	E_{FM}	E_{AFM}	$\Delta E_{NM\text{-}FM}$	$\Delta E_{AFM\text{-}FM}$	μ_B
Sn50%-Se0%	-118.951723	-119.126007	-119.125238	174.28	0.77	1.00
Sn100%-Se0%	-121.035401	-121.383791	-121.382230	348.39	1.56	2.00
Sn0-Se25%	-120.054787	-120.117556	-120.116101	62.77	1.46	0.96
Sn0%-Se75%	-127.192512	-127.258510	-127.257327	66.00	1.18	0.96

TOC
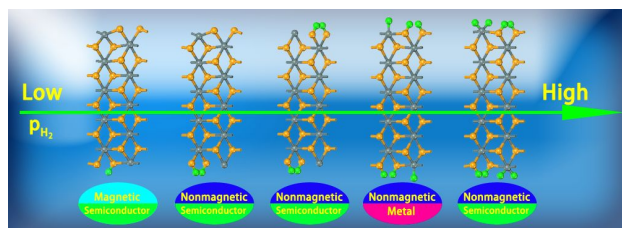
Versatile electronic phases and magnetic properties can be displayed through controlling the

partial pressure or chemical potential of hydrogen on $SnSe_2$ nanoribbon.